Academic Journal of Science and Technology
ISSN: 2771-3032 | Vol. 9, No. 1, 2024

Study of Multi-motor Synchronous Operation Based on Sliding Mode Virtual Spindle Adjacent Cross-coupling Control

Rui Zhang*, Yan Xia, Yang Chen, Kai Yang, Huizhu Li, Zetao Feng

Sichuan University of Science & Engineering, School of Automation and Information Engineering, Yibin, 643000, China
* Corresponding author: Zhang Rui (321081104118@stu.suse.edu.cn)

Abstract: Aiming at the problems of uneven parameter differences and load torque distribution, which cause the tracking accuracy and synchronization performance of the multi-motor control system to be reduced, a multi-motor system control strategy with sliding mode virtual spindle adjacent cross-coupling control is proposed. First, the feedback torque of each motor is regulated by establishing a virtual spindle to improve the coordination of the system. Secondly, a speed compensator is designed to couple each motor to improve the system synchronization. Meanwhile, the sliding mode control strategy is used for the control of a single motor. The robustness and tracking accuracy of the system are tuned up. The simulation experiment results show that compared with the sliding mode cross-coupling control, sliding mode adjacent deviation coupling control, and PI virtual spindle-adjacent deviation coupling control, the system has a small synchronization error, strong anti-interference ability, and realizes high-precision coordinated control of multiple motors.

Keywords: Permanent magnet synchronous motor, Multi-motor control, Virtual spindle control, Adjacent deviation coupling control, Sliding mode control.

1. Introduction

Multi-motor synchronous control is widely used in automobiles[1], wind power generation[2], coal mines[3], and other fields because it can provide a larger load drive and flexible motion mode for the system. In practical engineering, some factors, such as parameter differences in the motors and uneven distribution of torque to external loads, can reduced synchronization of multi-motor systems. the synchronization performance directly affects the stability and control accuracy of the whole system. Therefore, it is of great significance to research improving the synchronization of multi-motor control.

Multi-motor synchronization control mainly includes two kinds mechanical synchronization control and electrical synchronization control [4]. Mechanical synchronous control connects multiple motors through a mechanical master shaft to achieve the speed synchronization requirements. Mechanical synchronization control structure is simple and easy to implement, but there are problems such as low control accuracy and mechanical structure wear.

To solve the problems of mechanical synchronization control, scholars at home and abroad have proposed many electrical synchronization control algorithms, electrical synchronization control algorithms include coupled control and non-coupled control.

Uncoupled control mainly has master command control and master-slave control[5]. The master command control structure is that each motor shares the same input signal, and the control system of each motor is independent of each other. The master-slave control structure is that the speed output signal of the master motor is used as the input signal of the slave motor, and the slave motor can be regulated based on the output signal of the master motor [6]. When the load torque is consistent, the uncoupled control has good synchronization [7]. Since there is no coupling between the motors, when the load torque is not consistent due to external disturbances, it will cause the speed between the motors to be inconsistent and the system will lose synchronization.

The main types of coupling control are virtual spindle control [8], cross-coupling control [9], and deviation coupling control [10]. Virtual spindle control makes the multi-motor system keep synchronization by simulating the motion characteristics of the mechanical total axis [11]. However, there is the problem of time delay of the given signal and the system response is slow. Meanwhile, because there is no position controller in the virtual total axis control, the positional synchronization deviation that exists between the subsystems cannot be eliminated during the process of system startup and shutdown or when there is a random disturbance. Cross-coupling control adds speed error compensation based on parallel control to realize the coupling between motor control systems [12], but the cross-coupling control is only applicable to the synchronous control system of two motors, and the scope of application has limitations. Scholars have proposed deviation coupling control [13] by improving the cross-coupling structure, in which the speed output signal of each motor is multiplied by an appropriate scale factor after making a difference with the main motor, and then used as the speed compensation of each motor after summation. This control algorithm makes the system coupling degree high, any motor speed fluctuation can be transmitted to other motors so that the synchronization of the multi-motor control system is improved. As the number of motors in the system increases, the speed compensation module also increases, and the speed compensation module needs to consider the speed information of all motors, which makes the system arithmetic volume increase. Article [14] presents adjacent cross-coupling control decoupling by simplifying the speed compensator structure on the basis of deviation coupling. Adopting the adjacent motor speed as the compensator input signal reduces the number of input signals and improves the

operation efficiency of the system.

Therefore, a virtual spindle adjacent cross-coupling control structure is adopted in this paper. The torque information of all the motors is fed back to the virtual spindle, which is regulated through the virtual spindle, thus ensuring the coordinated operation of each motor. Each motor is compensated for the speed error of each motor through the adjacent cross-coupling structure, which improves the system coupling and ensures the system synchronization. At the same time, the use of an adjacent cross-coupling control structure simplifies the compensation structure of the system and reduces the system arithmetic. On this basis, the sliding mode controller is designed to control a single motor, which can further reduce the synchronization error of the system and improve the coordination and control accuracy of the system compared with the PI controller. Finally, the effectiveness of the control strategy is verified by simulation test results.

2. Design of Synchronous Control Structure for Multiple Permanent Magnet Synchronous Motors

2.1. Mathematical Model of Permanent Magnet Synchronous Motor

The following assumptions are made when establishing the mathematical model of a permanent magnet synchronous motor:

(1).Ignore space harmonics;

(2).Neglecting core losses;

(3).Neglecting magnetic circuit saturation;

The mathematical model on the two-phase rotating orthogonal coordinate system d-p is obtained by applying Clark's transform and Parker's transform to the voltages, currents and magnetic chains on the three-phase stator windings of a permanent magnet synchronous motor.

Stator voltage equation:

$$\begin{cases} u_d = R_s i_d + \dfrac{d\psi_d}{dt} - \omega\psi_q \\ u_q = R_s i_q + \dfrac{d\psi_q}{dt} + \omega\psi_d \end{cases} \tag{1}$$

The magnetic chain equation:

$$\begin{cases} \psi_d = L_d i_q + \psi_m \\ \psi_q = L_q i_q \end{cases} \tag{2}$$

The electromagnetic torque equation:

$$T_e = \frac{3}{2}\left[n_p \psi_m i_q + \left(L_d - L_q\right) i_d i_q \right] \tag{3}$$

In this paper, the permanent magnet synchronous motor is selected as the surface-mounted type, whose magnetic resistance of the shaft is equal to that of the shaft, and at this time, the electromagnetic torque equation is:

$$T_e = \frac{3}{2} n_p \psi_m i_q \tag{4}$$

Equations of motion:

$$\frac{d\omega}{dt} = \frac{n_p}{J}\left(T_e - T_L\right) \tag{5}$$

In the above equation, u_d, u_q, i_d, i_q, ψ_d, ψ_q are the stator voltage, stator current, and the components of the magnetic chain on the straight and intersecting axes; R_s is the stator resistance; L_d and L_q are the synchronous inductance on the straight and intersecting axes; n_p is the number of pole pairs of the motor; J is the rotational inertia; ψ_m is the magnetic chain of the permanent magnet; and ω is the angular velocity of the motor.

2.2. Virtual spindle-adjacent cross-coupling coordinated control strategy

The virtual spindle synchronization control is developed from the mechanical synchronization control, which has the physical characteristics of the mechanical spindle, and at the same time has the disadvantages of time delay of the given signal and slow system response. Therefore, the virtual spindle control structure combined with the neighboring cross-coupled control structure improves the system response speed, and to compensate for the speed error of each motor to improve the synchronization of the system. The multi-motor virtual spindle-adjacent cross-coupling control structure is shown in Figure 1.

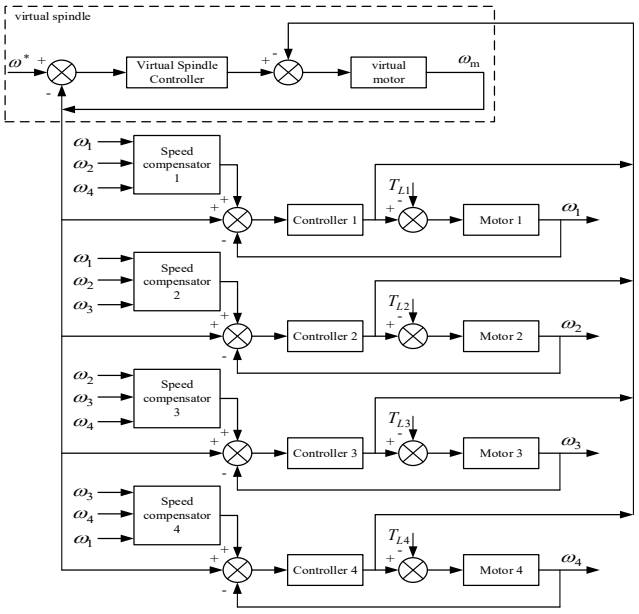

Figure 1. The multi-motor virtual spindle-adjacent cross-coupling control structure

When the system is running, the given rotational speed signal drives the virtual spindle to rotate, which in turn drives the slave axis motors to rotate. At this time, the virtual spindle equation of motion is:

$$T_m - \Sigma T_i = J\frac{d\omega}{dt} \tag{6}$$

Where: T_m is the output torque of the virtual spindle; T_i is the feedback torque of each motor; ω is the speed of the virtual spindle.

The virtual spindle output torque is related to the motor speed as:

$$T_m = k_m(\omega^* - \omega_m) \tag{7}$$

Where: ω^* is the given rotational speed; ω_m is the actual rotational speed of the virtual spindle; k_m is the elasticity coefficient of the virtual spindle.

2.3. Rotation speed compensator design

The structure of the adjacent cross-coupled control speed compensator is shown in Figure 2. Considering all single motors as master motors and adjacent motors as slave motors, it is only necessary to obtain the speed feedback from adjacent motors as input signals, make differences with the master motor respectively, and pass the gain parameter K and sum up as the speed compensation signal of each motor.

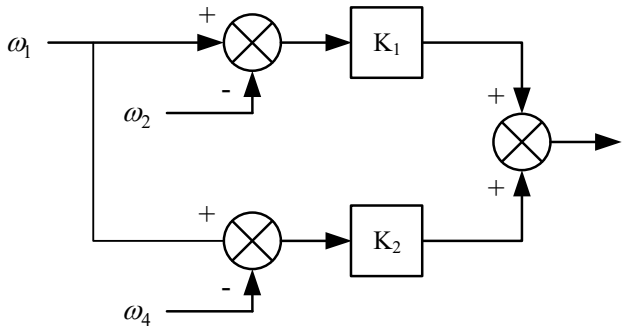

Figure 2. The structure of the adjacent cross-coupled control speed compensator

The compensation gain parameter K reflects the coupling degree of each subsystem, and the compensation gain parameter K should be selected regarding the rotational inertia of each slave axis. In this paper, the connection shaft between the motor and the virtual total axis is ignored, and the rotational inertia of the motor can be taken as the rotational inertia of the slave axis. To realize the synchronous and coordinated response of each motor speed, each compensation coefficient is normalized. Comparing the rotational inertia between the main motor and the neighboring motors, the maximum value (J_k) is selected as the reference inertia, and the rotational inertia of the remaining two motors is converted to the reference inertia for the conversion operation, to determine the compensation gain coefficients K of each motor.

$$K_i = \frac{J_i}{J_k} \tag{8}$$

3. Sliding Mode Control Strategy for Permanent Magnet Synchronous Motor

3.1. The quick-power reaching law

Mathematical expression for the traditional exponential convergence law:

$$\dot{S} = -\varepsilon \operatorname{sgn}(S) - KS \tag{9}$$

$$\operatorname{sgn}(x) = \begin{cases} 1, x > 0 \\ 0, x = 0 \\ -1, x < 0 \end{cases} \tag{10}$$

where: $\varepsilon > 0$, $K > 0$, sgn() is the sign function.

When the controlled quantity is far away from the sliding mode switching surface (S=0), the traditional exponential reaching law adopts the exponential way to converge; when the controlled quantity is closer to the sliding mode surface, the traditional exponential reaching law adopts the equal speed way to converge. Slip film gain ε is too large or too small, making the reaching speed faster or slower, the slip film system regulation process is unstable, causing the speed control system to jitter, so the traditional exponential reaching law of the motion performance is not good.

Aiming at the shortcomings of the traditional exponential-reaching law, the double-power reaching law (DPRL) increases a controlling factor based on the traditional exponential-reaching law. The double-power reaching law equation is[15]:

$$\dot{S} = -k_1 |S|^{w_1} \operatorname{sgn}(S) - k_2 |S|^{w_2} \operatorname{sgn}(S) \tag{11}$$

Where: $0 < \alpha < 1$.

Compared with the traditional exponential reaching law, the DPRL does not add new parameters, but only further utilizes the pre-existing data. When the system is far away from the sliding mode surface, when $S \to \infty$, $|S|^w \to \infty$, it can accelerate the speed of the control quantity converging to the sliding mode surface, so the reaching speed is much larger than the traditional exponential reaching law, which improves the response speed of the system. When the system converges to the sliding mode surface, the QPRL will be gradually reduced as the system is converging, $S \to 0$, $|S|^w \to 0$, which makes the system reach the sliding mode surface of the convergence speed less than the reaching speed of the traditional exponential reaching law, reducing the reaching movement through the inertia of the distance of the sliding mode surface, and when reaching the equilibrium state, the DPRL happens to be zero, to realize the sliding film variable structure control jitter suppression, and to improve the stability of the system. stability of the system.

3.2. Speed sliding mode controller design

The speed slip film controller requires the speed error to arrive and stabilize on the slide mold surface in a finite amount of time. The speed outer loop slip film controller output control quantity is i_q^*.

First, define the speed error:

$$e_\omega = \omega^* - \omega \tag{12}$$

Where: ω^* is the given speed; ω is the feedback speed. Define the speed sliding mode surface switching function:

$$S_\omega = e_\omega = \omega^* - \omega \tag{13}$$

If $S_\omega = 0$, the speed slip mode controller can stabilize on the slip mode switching surface the motor speed ω can

track a given speed ω^*.

Differential operations on the rotational speed sliding mode switching surface of Eq. (13) are obtained:

$$\dot{S}_\omega = \frac{d\omega^*}{dt} - \frac{d\omega}{dt} \tag{14}$$

This is obtained from the electromagnetic torque equation (4) and the motor motion equation (5):

$$\frac{d\omega}{dt} = \frac{n_p}{J}\left(\frac{3}{2}n_p\psi_m i_q - T_L\right) \tag{15}$$

This can be obtained by bringing equation (15) into equation (14):

$$\dot{S}_\omega = \frac{n_p}{J}\left(T_L - \frac{3}{2}n_p\psi_m i_q\right) \tag{16}$$

Bringing Eq. (16) into the QPRL Eq. (11) gives:

$$-k_{1\omega}\left|S_\omega\right|^{w_{1\omega}}\operatorname{sgn}(S_\omega) - k_{2\omega}\left|S_\omega\right|^{w2\omega}\operatorname{sgn}(S_\omega) = \frac{n_p}{J}\left(T_L - \frac{3}{2}n_p\psi_m i_q\right) \tag{17}$$

The speed slip mode controller expression can be obtained from equation (17):

$$i_q^* = \frac{2}{3n_p\psi_m}\left[\frac{J}{n_p}\left(k_{1\omega}\left|S_\omega\right|^{w_{1\omega}}\operatorname{sgn}(S_\omega) + k_{2\omega}\left|S_\omega\right|^{w_{2\omega}}\operatorname{sgn}(S_\omega)\right) + T_L\right] \tag{18}$$

According to the Lyapunov stability principle, it is known that to prove the stability of the rotational speed sliding mode controller, it needs to be satisfied:

$$\begin{cases} V(x) = \dfrac{1}{2}S^2 \\ \dot{V}(x) = S\dot{S} < 0 \end{cases} \tag{19}$$

Associative equations (11), (13), and (19) are used to construct the Lyapunov stabilization equations for the rotational speed sliding film controller:

$$\begin{aligned} \dot{V}_\omega = &-k_1\left|\omega^* - \omega\right|^{w_1}\cdot\operatorname{sgn}(\omega^* - \omega)\cdot(\omega^* - \omega) \\ &-k_2\left|\omega^* - \omega\right|^{w_2}\cdot\operatorname{sgn}(\omega^* - \omega)\cdot(\omega^* - \omega) \end{aligned} \tag{20}$$

The analysis of Eq. (20) shows that the first terms $\operatorname{sgn}(\omega^* - \omega)$ and $\omega^* - \omega$ have the same positivity, so it satisfies the Lyapunov stability condition $\dot{V}(x) < 0$. Therefore, the designed rotational speed sliding film controller can quickly converge to the sliding mode surface in a finite time, and the sliding mode controller is stable.

3.3. Current Sliding Mode Controller Design

The current equation of state of a permanent magnet synchronous motor in a two-phase rotating orthogonal coordinate system (d-q) is given by:

$$\begin{bmatrix} \dfrac{di_d}{dt} \\ \dfrac{di_q}{dt} \end{bmatrix} = \begin{bmatrix} -\dfrac{R_s}{L_d} & \dfrac{L_q}{L_d}\omega \\ -\dfrac{L_d}{L_q}\omega & -\dfrac{R_s}{L_q} \end{bmatrix}\begin{bmatrix} i_d \\ i_q \end{bmatrix} + \begin{bmatrix} \dfrac{1}{L_d} \\ \dfrac{1}{L_q} \end{bmatrix}\begin{bmatrix} u_d \\ u_q \end{bmatrix} + \begin{bmatrix} 0 \\ -\dfrac{1}{L_q}\omega\psi_m \end{bmatrix} \tag{21}$$

Define the current error:

$$\begin{bmatrix} e_{i_d} \\ e_{i_q} \end{bmatrix} = \begin{bmatrix} i_d^* - i_d \\ i_q^* - i_q \end{bmatrix} \tag{22}$$

Where: i_d^* is the stator current in the d-axis, and i_q^* is the stator current in the q-axis; i_d and i_q is the feedback current.

Define the current sliding mode surface switching function:

$$S = \begin{bmatrix} S_d \\ S_q \end{bmatrix} = \begin{bmatrix} e_{i_d} \\ e_{i_q} \end{bmatrix} = \begin{bmatrix} i_d^* - i_d \\ i_q^* - i_q \end{bmatrix} \tag{23}$$

A differential operation on the Eq. (23) current synovial section function gives:

$$\begin{bmatrix} \dfrac{dS_d}{dt} \\ \dfrac{dS_q}{dt} \end{bmatrix} = \begin{bmatrix} \dfrac{di_d^*}{dt} - \dfrac{di_d}{dt} \\ \dfrac{di_q^*}{dt} - \dfrac{di_d}{dt} \end{bmatrix} \tag{24}$$

The current state of a permanent magnet synchronous motor in a two-phase rotating orthogonal coordinate system (d-q) is obtained from equation (21) and equation (24):

$$\begin{bmatrix} \dfrac{dS_d}{dt} \\ \dfrac{dS_q}{dt} \end{bmatrix} = \begin{bmatrix} \dfrac{R_s}{L_d} & -\dfrac{L_q}{L_d}\omega \\ \dfrac{L_d}{L_q}\omega & \dfrac{R_s}{L_q} \end{bmatrix}\begin{bmatrix} i_d \\ i_q \end{bmatrix} - \begin{bmatrix} \dfrac{1}{L_d} \\ \dfrac{1}{L_q} \end{bmatrix}\begin{bmatrix} u_d \\ u_q \end{bmatrix} + \begin{bmatrix} 0 \\ \dfrac{1}{L_q}\omega\psi_m \end{bmatrix} \tag{25}$$

Bringing Eq. (25) into the fast power exponential convergence law Eq. (11) gives:

$$\begin{aligned} &\begin{bmatrix} -k_{1d}\left|S_d\right|^{w_1}\operatorname{sgn}(S_d) - k_{2d}\left|S_d\right|^{w2}\operatorname{sgn}(S_d) \\ -k_{1q}\left|S_q\right|^{w_1}\operatorname{sgn}(S_q) - k_{2q}\left|S_q\right|^{w2}\operatorname{sgn}(S_q) \end{bmatrix} = \\ &\begin{bmatrix} \dfrac{R_s}{L_d} & -\dfrac{L_q}{L_d}\omega \\ \dfrac{L_d}{L_q}\omega & \dfrac{R_s}{L_q} \end{bmatrix}\begin{bmatrix} i_d \\ i_q \end{bmatrix} - \begin{bmatrix} \dfrac{1}{L_d} \\ \dfrac{1}{L_q} \end{bmatrix}\begin{bmatrix} u_d \\ u_q \end{bmatrix} + \begin{bmatrix} 0 \\ \dfrac{1}{L_q}\omega\psi_m \end{bmatrix} \end{aligned} \tag{26}$$

The expression for the current slip film controller is obtained from equation (26):

$$\begin{aligned} \begin{bmatrix} u_d \\ u_q \end{bmatrix} = &\begin{bmatrix} R_s & -\omega L_q \\ \omega L_d & R_s \end{bmatrix}\begin{bmatrix} i_d \\ i_q \end{bmatrix} + \begin{bmatrix} 0 \\ \omega\psi_m \end{bmatrix} \\ &+ \begin{bmatrix} L_d \\ L_q \end{bmatrix}\begin{bmatrix} k_{1d}\left|S_d\right|^{w_1}\operatorname{sgn}(S_d) + k_{2d}\left|S_d\right|^{w2}\operatorname{sgn}(S_d) \\ k_{1q}\left|S_q\right|^{w_1}\operatorname{sgn}(S_q) + k_{2q}\left|S_q\right|^{w2}\operatorname{sgn}(S_q) \end{bmatrix} \end{aligned} \tag{27}$$

Prove the stability of the current slip film controller and construct the Lyapunov function:

$$V_i = \frac{1}{2}S^2 = \frac{1}{2}(S_d^2 + S_q^2) \tag{28}$$

Differentiation of Eq. (28) yields:

$$\dot{V}_i = \dot{S}_d S_d + \dot{S}_q S_q \tag{29}$$

Associative equations (11), (19), and (23) are used to construct the Lyapunov stabilization equations for the current sliding film controller:

$$\begin{aligned}\dot{V}_i = &-k_{1d}\left|i_d^* - i_d\right|^{w_{1d}} \operatorname{sgn}(i_d^* - i_d)(i_d^* - i_d) \\ &-k_{2d}\left|i_d^* - i_d\right|^{w_{2d}} \operatorname{sgn}(i_d^* - i_d)(i_d^* - i_d) \\ &-k_{1q}\left|i_q^* - i_q\right|^{w_{1q}} \operatorname{sgn}(i_q^* - i_q)(i_q^* - i_q) \\ &-k_{2q}\left|i_q^* - i_q\right|^{w_{2q}} \operatorname{sgn}(i_q^* - i_q)(i_q^* - i_q)\end{aligned} \tag{30}$$

The analysis of Eq. (20) shows that the first terms $\operatorname{sgn}(i^* - i)$ and $i^* - i$ have the same positivity, so it satisfies the Lyapunov stability condition $\dot{V}(x) < 0$. Therefore, the designed rotational speed sliding film controller can quickly converge to the sliding mode surface in a finite time, and the sliding mode controller is stable.

4. Simulation experiment and analysis

To verify the synchronization and effectiveness of the proposed sliding mode virtual spindle-adjacent cross-coupling control, the motor control simulation experiments of PI deviation coupling control, SMC deviation coupling control, SMC adjacent cross-coupling control, and SMC virtual spindle-adjacent cross-coupling control are constructed in the MATLB/Simulink platform, respectively. Four permanent magnet synchronous motors of the same model are selected as the controlled motors, and their corresponding parameters are slightly different considering the actual situation. The parameters of the four motors are shown in

Table **1**.

Table 1. The parameters of the four motors

	Stator resistance(Ω)	Armature inductance(H)	Flux linkage(Wb)	viscous damping(N·m·s)	Inertia(kg·m²)	pole pairs
Motor 1	1.5	0.012468	0.175	0.0003	0.000762	4
Motor 2	1.51	0.012466	0.1751	0.00031	0.000763	4
Motor 3	1.52	0.012468	0.1752	0.00032	0.000764	4
Motor 4	1.49	0.012468	0.1749	0.00033	0.000759	4

In the simulation test, the given speed is 500r/min and the load torque is 1 N·m. The load torque rises to 3 N·m in 20ms of steady-state operation and decreases to 2 N·m in 60ms of steady-state operation.

The motor speed under different control is shown in Figure 3, the motor speed of the SMC control structure enters the steady state in 8ms and has no overshooting, while the motor speed of the PI control structure has overshooting and vibration shaking phenomenon, and the steady state adjustment time is 5ms. when the load torque changes suddenly, the speed drop of the SMC control system is smaller than that of the PI controller, and it recovers to the steady state quickly, and the steady state recovery time is smaller than that of the PI control. the SMC control system is more robust than the PI control. The SMC control system is more robust than the PI control, improves the anti-interference performance of the system, and reduces the synchronization error of multiple motors.

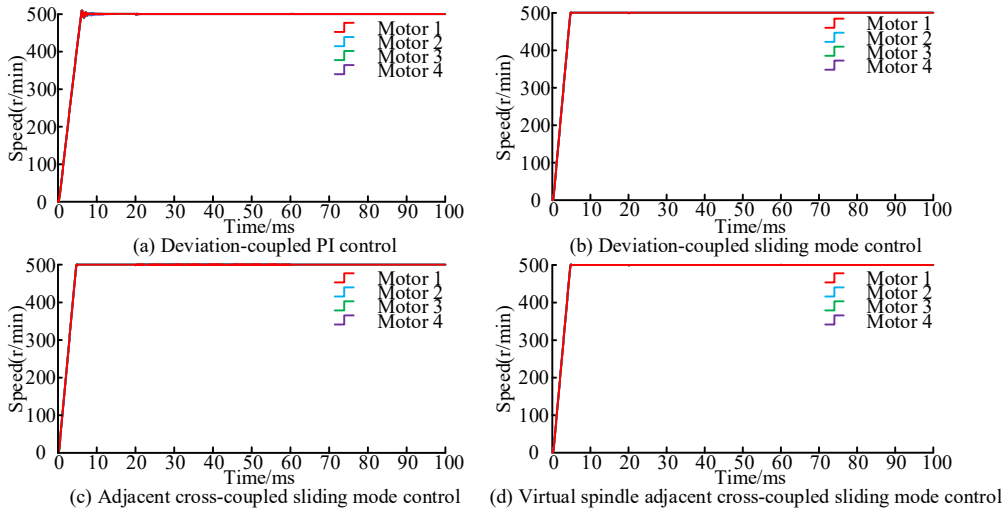

Figure 3. Speed comparison of motors with different control methods

The different controls corresponding to the motor error are shown in Figure 4, comparing Figure. 4-(a), 4-(b), 4-(c) and 4-(d). In the case where the synchronization error is always present, the PI deviation coupling control has the highest number of synchronization error oscillations and the largest synchronization error. The SMC virtual spindle-adjacent cross-coupling control has the smallest. The virtual spindle-adjacent cross-coupling control structure is the most sensitive

to inter-motor synchronization error and can adjust the inter-motor synchronization error in time.

The synchronization control effect will be compared to the synchronization error between motor 1 and motor 2, for example, as shown in Figure. 4-(d), the synchronization error of the virtual spindle-adjacent cross-coupling control structure is in the range of -0.004~0.001 rpm/min, and the maximum synchronization error is 0.004 rpm/min and tends to be close to 0. As shown in Figure 4-(c), the synchronization error of the adjacent cross-coupling control structure is in the range of -0.35 to 0.2 range. From Figure. 4-(b), the synchronization error of the deviation-coupled control structure varies in the range of -0.3 to 0.3. Comparing these three control structures, it can be seen that the virtual spindle-adjacent cross-coupling control structure has the smallest synchronization error, and the synchronization error can be precisely adjusted during the motor start-stop phase so that the synchronization error tends to zero.

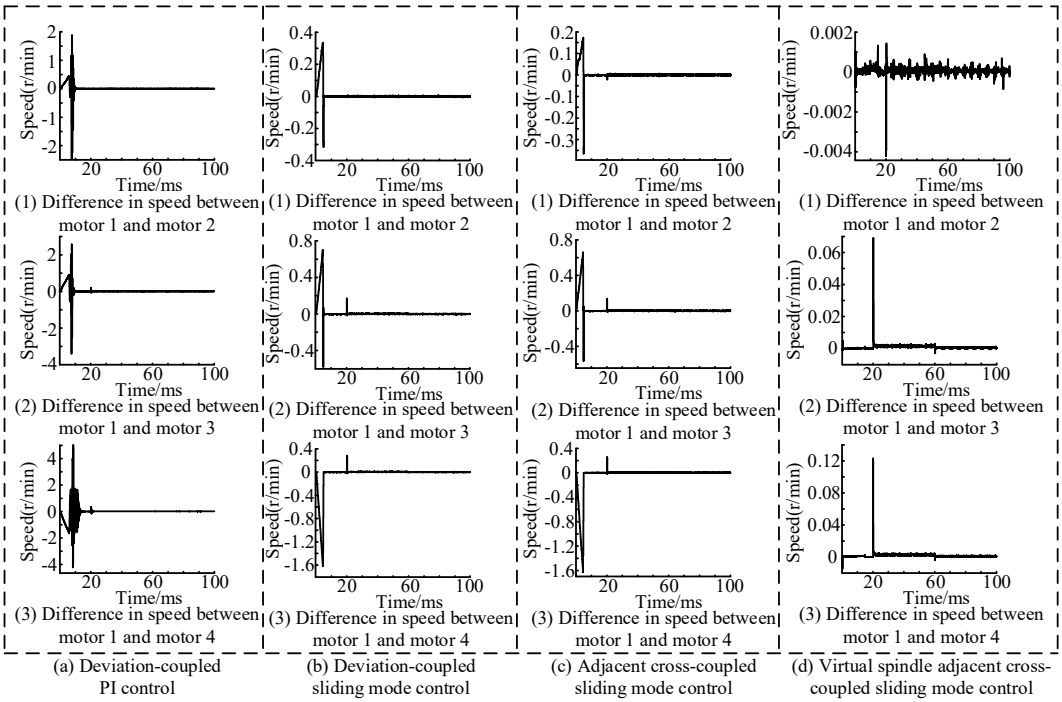

Figure 4. Comparison of speed errors of motors with different control methods

As can be seen from **Figure 5** and **Figure 6**, when the external load torque of the system changes, the synchronization error of the virtual spindle-adjacent cross-coupling control structure is the smallest, the system is almost free of oscillation, and the regulation time is the shortest and tends to be 0. In comparison, the systems of the adjacent cross-coupling control structure and the deviatoric coupling control structure are unable to reduce the system jitter vibration and exacerbate the phenomenon of jitter vibration during the regulation of synchronization error.

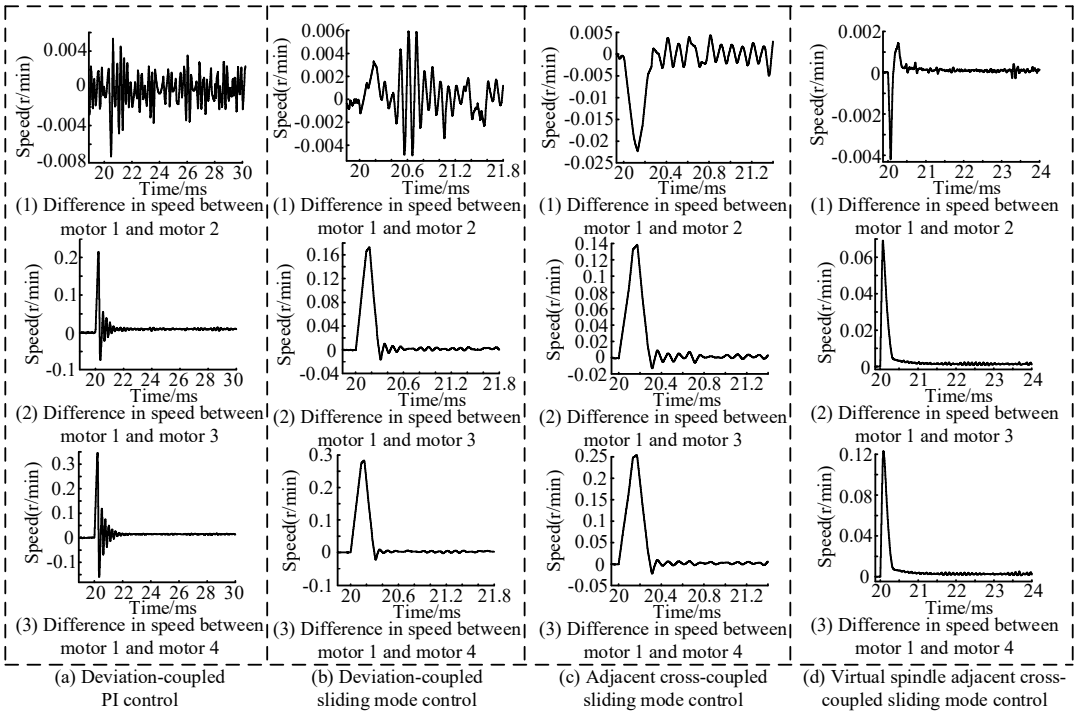

Figure 5. Comparison of speed errors of motors with different control methods (when load torque varies at 20ms)

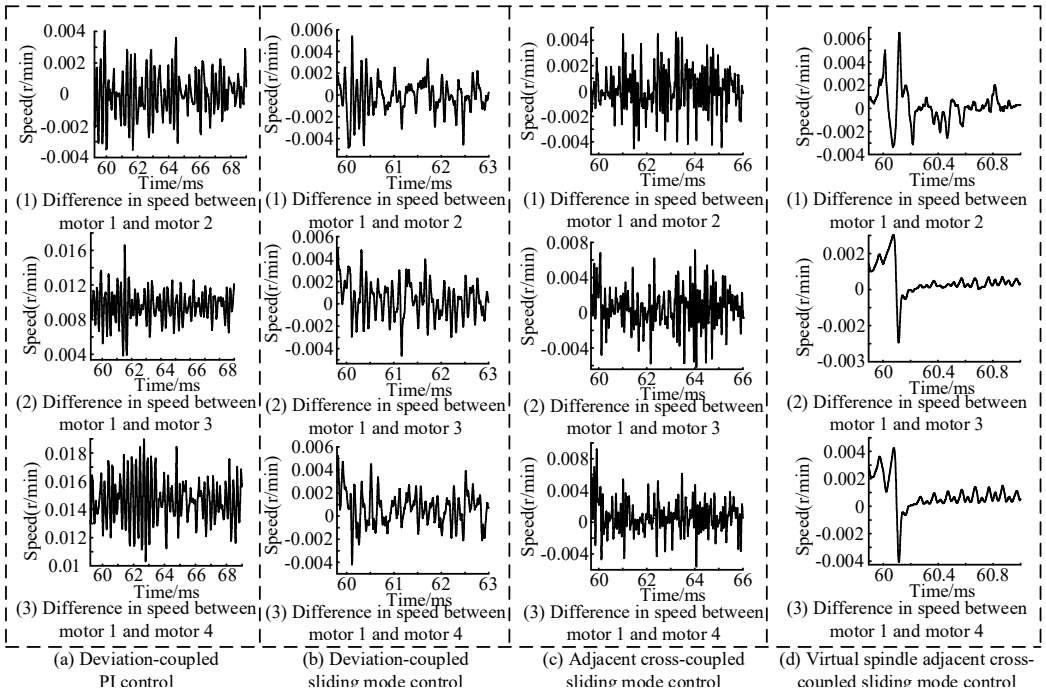

Figure 6. Comparison of speed errors of motors with different control methods (when load torque varies at 60ms)

5. Conclusion

Aiming at the shortcomings of the traditional multi-motor synchronous control system, such as synchronization error and poor following performance, this paper adopts the virtual spindle-cross-coupling control structure, designs the speed compensator to compensate the speed of each motor, and at the same time applies the sliding mode controller to the control of a single motor. The coordinated operation system of four synchronous motors is built by MATLAB/Simulink platform, and the simulation results show that the sliding mode control strategy improves the robustness and synchronization of the system to the differences in the motor parameters and load changes. Compared with the cross-coupled control structure and deviation-coupled control structure, the virtual spindle-cross-coupled control structure has the advantages of small synchronization error and good following performance, which reduces the synchronization error due to the parameter differences and makes the system have good coordinated control accuracy.

References

[1] Wu Yuhang, Xu Mingzhu. Improve Ring Coupling for Independent Drive Electric Multi-motor System[J]. Journal of Shijiazhuang Tiedao University (Natural Science Edition), 2023, 36(3):112-118.

[2] Fang Tao, Gao Dezong. Research on Multi-megawatt Direct Drive Wind Power System and Generator Control[J]. CFHI TECHNOLOGY, 2013(01):16-19.

[3] Yang Bin. Design and Application of Multi motor Intelligent Control System for Coal Mine Belt Conveyor[J]. Mechanical Management and Development, 2023, 38(05):182-184.

[4] LI Dongliang, MIAO Zhongcui, WANG Zhihao, et al. Synchronous Flux Weakening Control Strategy of Multi-MotorSystem Based on Model Prediction[J]. Electric Machines & Control Application 2019,46(11):7-12.

[5] Xin Li, Wenlin Zhou, Dan Jia, et al. A Decoupling Synchronous Control Method of Two Motors for Large Optical Telescope[J]. IEEE Transactions on Industrial Electronics, vol. 69, no. 12, pp. 13405-13416, Dec. 2022.

[6] F. J. Torres, G. V. Guerrero, C. D. García, et al. Master-Slave Synchronization of Robot Manipulators Driven by Induction Motors[J]. IEEE Latin America Transactions, vol. 14, no. 9, pp. 3986-3991, Spe. 2016.

[7] Dongming Xiao, Xuejun Li, Kuanfang He. Power Balance of Starting Process for Pipe Belt Conveyor Based on Master-Slave Control[J]. IEEE Access, vol. 6, pp. 16924-16931, 2018.

[8] Xiang Gu, Zhaoping Du, Weiran Wang, et al. Multi-motor underwater coordinated control system based on virtual spindle[J]. 2020 Chinese Automation Congress (CAC), Jan. 2021.

[9] Zuo Ting, Lu Hong, Fan Wei, et al. Research on Dual Drive Synchronization Performance Based on Virtual Shaft Control Strategy[J]. 2017 2nd International Conference on Robotics and Automation Engineering (ICRAE), 2017.

[10] Changlin Zhu , Qunzhang Tu, Chengming Jiang, el al. A Cross Coupling Control Strategy for Dual-Motor Speed Synchronous System Based on Second Order Global Fast Terminal Sliding Mode Control[J]. IEEE Access, vol. 8, pp. 217967-217976, 2020.

[11] Zheng Li, Qingshan Zhang, Yiding Zhu, et al. Control Strategy of Biaxial Variable Gain Cross-Coupled Permanent Magnet Synchronous Linear Motor Based on MPC-MRAS[J]. IEEE Transactions on Industry Applications, vol. 58, no. 4, pp. 4733-4742, July. 2022.

[12] Guoliang Zhong, Zhizhong Shao, Hua Deng, et al. Precise Position Synchronous Control for Multi-Axis Servo Systems[J]. IEEE Transactions on Industrial Electronics, vol. 64, no. 5, pp. 3707-3717, May. 2017.

[13] Yanjuan Wu , Yanbin Cheng, Yunliang Wang. Research on a Multi-Motor Coordinated Control Strategy Based on Fuzzy Ring Network Control. IEEE Access, vol. 8, pp. 39375-39388, 2020.

[14] Lu Zi-shuai, Cai Wei, Zhao Jingyi, et al. Active Disturbance Rejection Control for Adjacent Cross Coupling Synchronization of Hydraulic System Group [J]. Chinese Hydraulics & Pneumatics, 2020(08): 29-34.

[15] Yang Guangyu., Chen Siyi. Piecewise fast multi-power reaching law: Basis for sliding mode control algorithm [J]. Measurement and Control, 2020, 53(9-10):1929-1942.